ChemComm

Accepted Manuscript

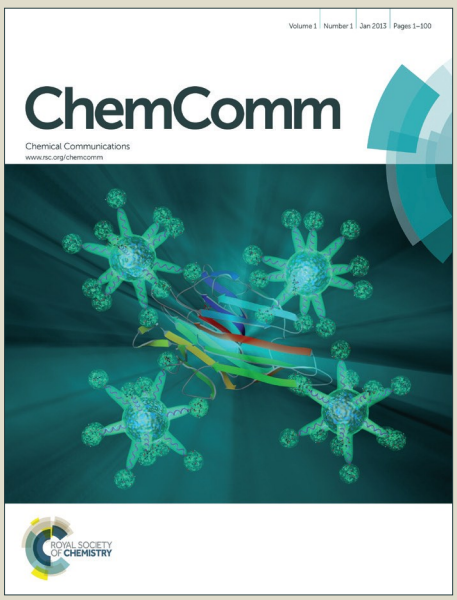

ROYAL SOCIETY OF CHEMISTRY

www.rsc.org/chemcomm

Chemical Communications RSCPublishing

COMMUNICATION

Implantable Nonenzymatic Glucose/O_2 Micro Film Fuel Cell Assembled with Hierarchical AuZn Electrodes

Cite this: DOI: 10.1039/x0xx00000x

Received 00th January 2012,
Accepted 00th January 2012

DOI: 10.1039/x0xx00000x

www.rsc.org/

Hui-Bog Noh,[a] M. Halappa Naveen,[a] Yong-Jin Choi,[a] Eun Sang Choe[b] & Yoon-Bo Shim*[a]

Hierarchical AuZn dendrite revealed electrocatalytic properties towards the glucose oxidation and the four-electron O_2 reduction. The micro fuel cell using AuZn electrodes generated power density of 2.07 and 0.29 mWcm^{-2} for glucose and human whole blood. The micro film cell implanted into the rat brain produced ~0.52 V continuously operating more than 18 days.

Biomass is an ideal alternative to fossil fuels.[1] Of these, glucose is one of the most interesting biomass fuels, because it is renewable, cheap, abundant, nontoxic, non-flammable, and easily handled and obtained. Furthermore, it is an excellent candidate fuel for implantable fuel cells (FCs) in animal bodies and body fluids.[2,3] Attempts have been made to research implantable glucose biofuel cells (BFCs) based on enzyme catalysts, such as glucose oxidase,[4,5] although such FCs have exhibited insufficient durability and lack of reproducibility of the enzymatic systems. Although the lifetime of enzyme based BFCs can be somewhat enhanced using conducting-polymer-based enzyme electrodes,[6] it is expected that FCs driven by nonenzymatic oxidation of glucose will be more useful. The methods developed for nonenzymatic glucose oxidation suffer from two fundamental problems,[7] however. One arises from the low efficiency of the oxidation reaction caused by slow rates, and the other is associated with electrode surface poisoning by adsorbed intermediates or products.[8] Thus, they are difficult to be used for continuous power source. Consequently, the development of new electrode materials that can efficiently catalyze the glucose oxidation and the oxygen reduction in mammals is an important goal of current implantable BFC studies. Recently, metal dendrites have received extensive attention in the fields of biology, chemistry, and physics owing to their unique geometry and potential applications in FCs[9-12] and biosensors.[13,14] Although numerous metals have been employed to generate dendrite,[13,15] the applications of hierarchical AuZn as FC and BFC electrodes have not been reported much, so far. The aim of the present study is to synthesize new hierarchical bimetal catalysts (AuZn, AuNi, and AuCo) and to apply them for the implantable glucose/O_2 FCs (GOFCs).

AuZn, AuNi, and AuCo dendrites were electrochemically prepared, their preparation conditions and analytical parameters were optimized, and the catalytic activity for fuel cell reactions was analyzed (see Electronic Supplementary Information (†ESI), materials and methods section). Among these bimetal dendrites, the AuZn dendrite was extensively studied, because it showed the best performance for the FC reactions compared with the other Au-transition metal bimetals. The AuZn dendrite was prepared at the following optimized condition; The dendrites were prepared in a O_2 purged 0.1 M Na_2SO_4 solution containing 10.0 mM $HAuCl_4 \cdot 3H_2O$ and 30.0 mM $ZnCl_2$, $NiSO_4$, and $CoCl_2 \cdot 4H_2O$, respectively. The pH was maintained at 4.0 using NaOH. The deposition potentials for AuZn, AuNi, and AuCo dendrites were -500.0, -600.0, and -700.0 mV, respectively, for 1000.0 s. The mixed solution was purged with N_2 gas for 30 min before the electrodeposition process. Then, the electrodes were washed successively with 0.1 M HCl, acetone, ethanol, and water several times. The experimental parameters were optimized in terms of the concentration of analytes, deposition time, deposition potential, and pH, which affect dendrite formation and catalytic activity.

Since the surface morphologies of all as-prepared bimetals are the same, that of the AuZn bimetal electrode is discussed as a typical example based on scanning electron microscopy (SEM) in the present study, as shown in Fig. 1(A), which was distinguishable by the presence of side branch tips split from the main chain (images of AuNi and AuCo are not shown). Simultaneously, energy dispersive X-ray spectroscopy (EDXS) analysis was also performed to determine the composition of the AuZn dendrite. The spectrum displayed in Fig. 1(B) (where the inset is an SEM image of the sample) shows that the ratio of the atomic components of the bimetal, Au:Zn, is 51.88:48.12. To obtain further information on the distribution of Au and Zn during the dendrite growth, spectra and images were acquired using time-of-flight secondary ion mass spectroscopy (TOF-SIMS) in a positive mode. Fig. 1(C) shows the TOF-SIMS images of the dendrite for (a) Au^{3+} (m/z 590.90), (b) Zn^{2+} (m/z 130.84), and (c) overlaid Au^{3+} and Zn^{2+} ions. Au^{3+} and Zn^{2+} were chosen due to their obvious signals, and these TOF-SIMS images present similar topographies and morphologies to those observed in the SEM image. In this case, the analysis area is 50.0 μm x 50.0 μm, and the bright colors on the TOF-SIMS images correspond to the higher intensities of each species. We can clearly

observe that both of these elements are distributed homogeneously in bimetal dendrite shapes. The X-ray diffraction (XRD) patterns, obtained for Zn, Au, and AuZn dendrites [(a-c) respectively in Fig. 1(D)], contain typical Au and Zn dendrite peaks at the 2θ values of 38°, 44°, 64°, and 77°; and 36°, 39°, 43°, 54°, 70°, 71°, and 78°, respectively. The XRD pattern of the AuZn dendrite [(c) in Fig. 1(D)] contains high intensity peaks associated with both metals. Au and Zn are both homogeneously dispersed among each other. Overall, the homogeneous distributions of Au and Zn in the porous bimetal dendrites are expected to promote catalytic oxidation of glucose and reduction of O_2. Compared to the corresponding pure Au dendrite, the Au peaks in the XRD pattern of the bimetal are slightly shifted and broadened. The index peaks, assigned as (111), (200), (220), and (311), identify the material as face-centred cubic (fcc) and appear at diffraction angles corresponding to electrodeposited fcc Au and Zn, respectively.

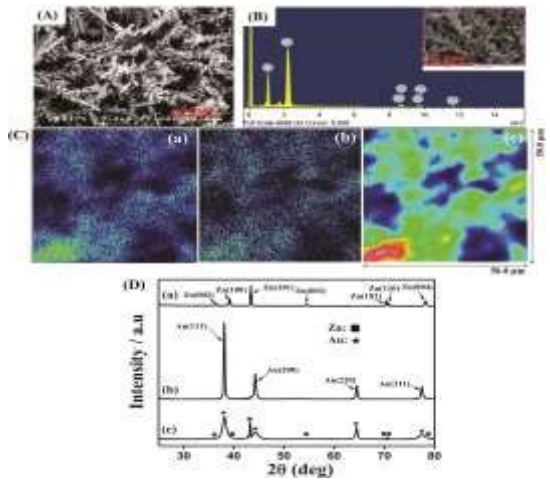

Fig. 1. (A) SEM image of AuZn dendrites. (B) EDXS spectrum and image (inset) of the dendrite. (C) TOF-SIMS images of dendrites: (a) Au^{3+}, (b) Zn^{2+}, and (c) two-colour overlay of the Au^{3+} and Zn^{2+} ions (field of view: 50.0 µm x 50.0 µm). (D) XRD spectra of (a) Zn, (b) Au, and (c) AuZn dendrites.

The catalytic characteristics were compared for both the oxygen reduction reaction (ORR) and glucose oxidation reactions, where the bimetal components were chosen due to the similar preparation conditions and catalytic properties for the FC reactions. The electrocatalytic activity of all the as-prepared materials towards the ORR was investigated in O_2 and N_2 saturated solutions. As shown in †ESI Fig. S1, the onset potentials of O_2 in linear sweep voltammograms (LSVs) are -87.5 mV for Pt, -66.4 mV for Au dendrite, -47.7 mV for AuZn dendrite, -48.9 mV for AuNi dendrite, and -59.6 mV for AuCo dendrite electrodes. The AuZn dendrite revealed the best performance compared with the other Au-transition-metal bimetal, so its FC reactions were extensively studied in the subsequent experiments. To elucidate the kinetic characteristics of the ORR, hydrodynamic voltammograms (HVs) using a rotating disk electrode (RDE) were collected for the O_2 reduction process in a saturated 0.1 M NaOH solution [Fig. 2(A) and (B)]. For instance, the onset potential of the AuZn dendrite electrode is shifted positively to +85.1 mV, and the diffusion current at -700.0 mV is ~1.3 times larger than that of the Au dendrite electrode (with the onset potential shifted by +38.2 mV). The number of transferred electrons (n) per O_2 molecule involved in the ORR was determined by using the Koutecky-Levich equation [Equations (1) and (2)],[16]

$$\frac{1}{J} = \frac{1}{J_{kin}} + \frac{1}{J_{diff}} = \frac{1}{J_{kin}} + \frac{1}{B\sqrt{\omega}} \quad (1)$$

$$B = 0.62nFD^{2/3}\nu^{-1/6}C \quad (2)$$

where n is the number of electrons transferred during the ORR, F is the Faraday constant, D is the diffusion coefficient of O_2 in the 0.1 M NaOH electrolyte (D = 1.9 × 10^{-5} cm^2s^{-1}), C is the bulk concentration of O_2 (C = 1.2 × 10^{-3} $mMcm^{-3}$), and ν is the kinetic viscosity of the electrolyte (ν = 1.0 × 10^{-2} cm^2s^{-1}). The n values, which are dependent on the potential, were observed to be 3.5, 2.6, 3.9, 3.5, and 3.1 for pure Pt, and Au, AuZn, AuNi, and AuCo dendrite electrodes at ~-500.0 mV, respectively [inset of Fig. 2(A)]. The results demonstrate that the electrocatalytic activity of the AuZn dendrite towards the ORR is somewhat higher than those of metal and bimetal dendrites in terms of the onset and half-wave potentials. The number of electrons (n value) for the ORR at the AuZn bimetal dendrite electrode was observed to be always higher than those at the pure Au dendrite and pure Pt electrodes over the potential range that was probed. This observation indicates that the AuZn bimetal dendrite structure is a more efficient ORR electrocatalyst than pure Au electrode, and its ORR process proceeds *via* a four-electron transfer pathway.[17] The Koutecky-Levich plot that was obtained to determine the kinetic proficiency of the test electrode displayed good linearity, with the slope remaining approximately constant over the entire potential range used. This might be related to the oxidation of $Au(OH)_3$ (formed on the Au surface in the alkaline electrolyte) to a higher-valence oxyhydroxide. HVs were collected using a RDE at various rotation speeds to obtain further insight into the ORR performance of the AuZn dendrite [Fig. 2(B)]. The voltammograms show that in contrast to the bare Pt and Au dendrite electrodes, the AuZn dendrite deposited in the disk electrode region facilitates interaction with the electrolyte. At all rotation speeds, the limiting currents for the ORR at the AuZn dendrite electrode were higher than those for the ORR at the bare Pt and Au dendrite electrodes (not shown). In addition, RDE experiment for ORR was performed in physiological pH medium (pH 7.4, containing 0.14 M Cl^-, 25 ^oC). As shown in †ESI Fig. S2, the increasing current density was observed with increasing rotation rates similar to that in alkaline solution.

Cyclic voltammograms (CVs) of AuZn and (inset) Au dendrites in blank (black) and 10.0 mM glucose-containing (C) NaOH and (D) physiological conditions (pH 7.4, containing 0.14 M Cl^-, 37.5 ^oC) (red) are displayed in Fig. 2. CVs for other electrode materials are shown in †ESI Fig. S3: (A) bare glassy carbon (GC), (B) bare Au, (C) AuNi, and (D) AuCo dendrite electrodes. CVs recorded for the Au dendrite exhibit redox peaks at +337.3/+107.3 and -225.9/-305.4 mV.[18] A set of redox peaks for the AuZn dendrite additionally appears at -686.4/-754.1 mV, which correspond to redox processes of Zn. The redox peaks corresponding to the Au redox process itself of the AuZn dendrite appear at +551.3/+11.7 and -491.9/-611.2 mV, where the latter pair is a consequence of the oxidation of glucose to gluconolactone and other minor products (Fig. 2(C)). Otherwise, CVs recorded for Au dendrite under physiological conditions exhibit a set of redox peaks at +265.8/+193.1 mV and an oxidation peak at +452.4 mV. On the other hands, two pairs of redox peaks for polymer (Nafion/polyurethane) coated on AuZn dendrite appear at -350.2/-533.7 and +173.0/-3.6 mV, where the former is responsible to a redox process of Zn, and the latter is to Au in a blank buffer solution as shown in Fig. 2(D). The dissolution of Zn ion from polymer/AuZn surface was confirmed using EDXS, there is no dissolution of Zn in the physiological condition (0.4% Zn was dissolved, which is within the experiment error range), while most of Zn is dissolved from the AuZn surface in the acidic medium (98.8% Zn was dissolved).

The number of electrons involved in the glucose oxidation reaction at the AuZn bimetal electrode was determined by employing controlled potential coulometry, and the oxidation products were analyzed using high-performance liquid chromatography-electrospray ionization mass spectrometry (HPLC-

ESI MS) (see †ESI Fig. S4). The coulometric experiment was performed in 5.0 mL blank solution (0.1 M NaOH) and separately in the same solution containing 1.0 µM glucose. The potential of +400.0 mV was applied for the glucose oxidation over 150 min. In both cases, charges (Q) were obtained of -24.4 and -33.1 mC for 120 min, respectively. The anodic products of glucose oxidation at the AuZn dendrite electrode were shown to be gluconolactone, amounting to 41% (2-electron oxidation product, EOP), with other minor products such as oxalate (15 %, 18-EOP), formate (3%, 12-EOP), glyoxatylate (8%, 12-EOP), glycolate (1%, 6-EOP), glucalate (25%, 6-EOP), 2-keto-gluconate (6%, 4-EOP), and glycelate (1%, 4-EOP).

Surface analysis of the dendrite was carried out using X-ray photoelectron spectroscopy (XPS) to confirm the composition and oxidation states of the AuZn bimetal. The XPS spectra displayed in †ESI Fig. S5 contain corresponding peaks of the dendrite associated with (A) the survey spectrum, (B) Zn $2p_{3/2}$, and (C) Au $4f_{(5/2, 7/2)}$. The pristine dendrite (I) displays peaks at 1021.2 eV and at 88.2 and 84.3 eV, corresponding to Zn and Au, respectively,[19] which indicates that both Zn and Au exist in their reduced metallic states. During the glucose oxidation and O_2 reduction reactions, new XPS peaks appear at approximately 1022.2 eV and at 89.4 and 85.5 eV, which correspond to the respective peaks of ZnO and Au_2O_3. As can be seen in (III) and (IV), the peak intensities corresponding to ZnO and Au_2O_3 increase as the glucose oxidation and O_2 reduction reactions continue, in contrast to the behaviour of the blank solution (II and IV).

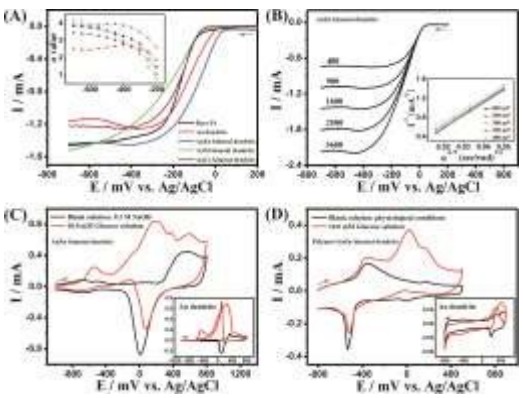

Fig. 2. (A) HVs recorded for the ORR at bare Pt (black), Au (red), AuZn (blue), AuNi (green), and AuCo (purple) electrodes in O_2 saturated 0.1 M NaOH at 10.0 mVs^{-1} at 1600 rpm; inset: plot of the transferred electron number *vs.* voltage. (B) HVs for the ORR of AuZn dendrite according to the rotation rates (rpm: 400, 900, 1600, 2500, and 3600); inset: Koutecky-Levich plots. CVs recorded for AuZn, polymer/AuZn, and Au (inset) dendrite electrodes in blank (black) and 10.0 mM glucose (red line) in (C) 0.1 M NaOH and (D) physiological conditions (pH 7.4, containing 0.14 M Cl^-, 37.5 ^oC).

Representative applications of AuZn dendrite in a FC and a biosensor were demonstrated for standard glucose and blood samples. Fig. 3(A) contains a schematic representation of a GOFC composed of a pair of AuZn electrodes separated in 100 µm gap by paper. The cell is composed of two compartments in which an O_2 and a glucose-containing solution are externally connected in a closed loop with a FC system, which was operated at open-circuit voltage. Fig. 3(B) shows the cell voltage and power density versus current density curves for the cell. The performance of the cell containing 100.0 mM glucose at 25 ^oC revealed the following characteristics: cell voltage of 0.91 V, current density 2.83 $mAcm^{-2}$, and power density 1.63 $mWcm^{-2}$. Besides glucose, human whole blood (blood glucose level of 108.5 mg/dL, 25 ^oC) and 5.0 mM test glucose solutions (25 and 37.5 ^oC) were used as the anodic fuel. In this case, the cell performance had the following characteristics: cell voltage of 0.59, 0.62, and 0.63 V, current density 1.21, 1.45, and 1.50 $mAcm^{-2}$, and power density 0.29, 0.38, and 0.41 $mWcm^{-2}$. The power density obtained using a glucose test solution is 11.4 times higher than the previously reported one using a nonenzymatic-catalyst-based glucose/O_2 system.[20] This might be because a total number of electrons of 18 ± 1.5 is involved in the glucose oxidation reaction at AuZn. The cell voltage and power density curves as functions of the temperatures (20 - 75 ^oC) and the glucose concentrations (500.0 nM - 150.0 mM) was obtained under alkaline solution (0.1 M NaOH), where the maximum power density was 2.07 $mWcm^{-2}$ at 50 ^oC (see †ESI Fig. S6(A and B) and Table S1). In addition, *in vitro* control experiments were performed under physiological conditions (pH 7.4, containing 0.14 M Cl^- and 37.5 ^oC) in the glucose concentrations between 0.01 and 50.0 mM. In this case, the power density was 0.41 $mWcm^{-2}$ at 5.0 mM glucose (RSD (n = 3) was <7.3%) (see †ESI Fig. S6(C and D) and Table S1).

The current is proportional to the glucose concentration, which is potentially applicable for continuous *in vitro* glucose sensor. The maximum cell voltage, current density, and power density at a glucose concentration of 100.0 mM and 50 ^oC are 0.98 V, 3.50 $mAcm^{-2}$, and 2.07 $mWcm^{-2}$, respectively. Long-term stability testing of a FC containing the dual AuZn dendrite electrodes was carried out over 832 h, where the power density slowly decreased to a 28.9% loss by 711 h operation.

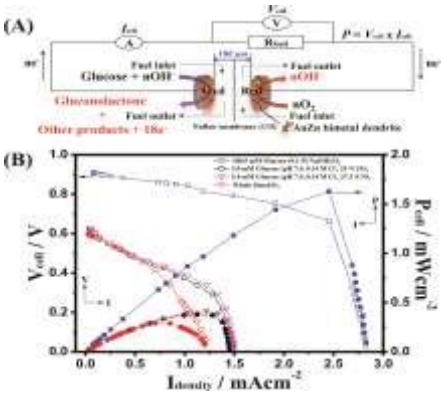

Fig. 3. (A) Schematic diagram of a GOFC system. (B) *I-V* and *I-P* curves for glucose in 0.1 M NaOH (25 ^oC), whole blood (25 ^oC), and physiological conditions (pH 7.4, 25 and 37.5 ^oC).

The performance of micro GC (cell size: 8 mm x 4 mm, diameter: 5.0 mm) and micro film (cell size: 4 mm x 6 mm, thickness: 1 mm, diameter: 3.0 mm) FCs implanted in Wistar rats was evaluated using a pair of two carbon screen-printed micro film electrode (SPME) and GC. A biocompatible FC with bimetal on the GC was implanted in the (†ESI Fig. S7(A)) abdominal cavity, and FCs with the micro film electrodes (a) subcutaneous layer of neck, and (b) brain of a rat, separately (Fig. 4(A)). The implanted FC measured power density while the rat was held in position on a stereotaxic frame (Fig. 4(A)a). A cell composed of dendrite-deposited GC electrode as anode and cathode (AuZn bimetal) separated with polymer film was wired using brass. The pair of electrodes was wrapped with perforated silicone tube (inset of †ESI Fig. S7(A)). A micro film FC assembled with the SPMEs was also formed and insulated using tape (inset of Fig. 4(A)). The possibility of gliosis caused by implantation of the electrode was verified using Nissl staining (data not shown). The voltage outputs from the FCs implanted into rat were measured at open circuit using a multimeter, and they were determined to be 0.54, 0.52, and 0.55 V for the GC and SPMEs, respectively. Fig. 4(B) shows *I-V* and *I-P* curves for the micro film cells. The cells (inset of

†ESI Fig. S7(B)) in the abdominal cavity, (Fig. 4(A(a)) subcutaneous layer of neck, and (Fig. 4(B(b)) brain of rat produced cell voltages of 0.54, 0.52, and 0.55 V, current density of 0.52, 0.33, and 0.47 $mAcm^{-2}$, and power density of 0.11, 0.10, and 0.11 $mWcm^{-2}$, respectively. The *in vivo* performance (power density 0.11 $mWcm^{-2}$) of the implantable micro film FCs composed of AuZn dendrite was lower than that obtained for the *in vitro* blood sample (power density 0.29 $mWcm^{-2}$) using the same electrode, because of the different glucose concentration. Fig. 4(C) shows long-term stability test of implanted micro film FCs, where the cell voltage stayed between 0.55 and 0.52 V, but the current density showed a slight decrease after two days and in successive measurement remained stable between 0.43 and 0.39 $mAcm^{-2}$. The micro film FC implanted in the rat brain remains stable for more than 18 days. The cell performance was compared with other literatures (see †ESI Table S2).

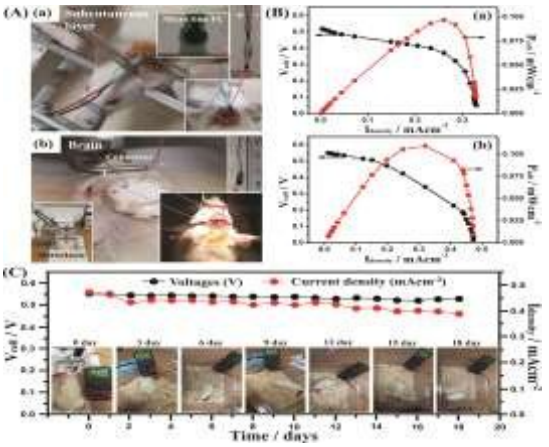

Fig. 4. (A) Micro film FCs implanted in the (a) subcutaneous layer of neck and (b) brain of rat (polymer/AuZn with SPMEs). Electrical connection of the FC in Wistar rats; the output wires are fixed to the stand. (B) *I-V* and *I-P* curves of FCs in neck and brain. (C) Long-term stability test for 18 days in the brain.

The obtained power density of the proposed implantable GOFC represents a promising solution to several issues for electronic medical devices. The FC that we report produces significant levels of energy at a single location and hence could be utilized as the power source for implanted devices dedicated to medical monitoring. Further optimization of our FC could be expected to provide opportunities for other medical applications such as multiple-lead cardiac resynchronization therapy (promising for some types of heart failure) or peripheral nerve stimulation (e.g. for pain control). In the case of peripheral nerve stimulation, several small FCs could be used instead of the currently implanted bundle of wires from a single sealed battery.

In conclusions, Au-M (M: Zn, Ni, and Co) dendrites were successfully prepared by using the potential step method, which possess homogenous, and crystal hierarchical structure. These bimetal dendrites were used as dual catalysts for the glucose oxidation and the ORR. The most excellent catalytic activities in the glucose oxidation and ORR processes were observed on the AuZn dendrite; the performance for FC was much higher than that of pure Au and/or Pt electrodes. Importantly, the results show that electricity can be successfully generated from both the glucose/O_2 (2.07 $mWcm^{-2}$ at 50 °C) and the whole blood/O_2 fuels system using the AuZn dendrite. The micro film FC implanted in the rat brain remains stable for more than 18 days. In addition, the current of FC is directly proportional to the glucose concentration, which is potentially applicable for a continuous *in vivo* glucose sensor.

This work was supported by the National Research Foundation of Korea (NRF) grant funded by the Korea government (MSIP) (No. 20100029128).

Notes and references

[a] Department of Chemistry and Institute of Biophysio Sensor Technology (IBST), Pusan National University, Busan 609-735, South Korea.
Tel: +82-51-510-2244; E-mail: ybshim@pusan.ac.kr;
[b] Departments of Biological Sciences, Pusan National University, Busan 609-735, South Korea.

† Electronic Supplementary Information (ESI) available: Materials and methods, LSVs and CVs recorded for the Au-M in glucose solutions, HVs recorded for the polymer/AuZn in the O_2 saturated physiological medium, XPS analysis, the optimization of the experimental parameters, and FC implanted in the abdominal cavity. See DOI: 10.1039/c000000x/

1. G. W. Huber and A. Corma, *Angew. Chem., Int. Edit.*, 2007, **46**, 7184.
2. V. Oncescu and D. Erickson, *Sci. Rep.*, 2013, DOI: 10.1038/srep01226.
3. S. Kerzenmacher, J. Ducree, R. Zengerle and F. von Stetten, *J. Power Sources*, 2008, **182**, 1.
4. S. E. Ichi, A. Zebda, A. Laaroussi, N. Reverdy-Bruas, D. Chaussy, M. N. Belgacem, P. Cinquin and D. K. Martin, *Chem. Commun.*, 2014, **50**, 14535.
5. A. Zebda, S. Cosnier, J. -P. Alcaraz, M. Holzinger, A. Le Goff, C. Gondran, F. Boucher, F. Giroud, K. Gorgy, H. Lamraoui and P. Cinquin, *Sci. Rep.*, 2013, DOI: 10.1038/srep01516.
6. H. -B. Noh, M. -S. Won, J. Hwang, N. -H. Kwon, S. C. Shin and Y. -B. Shim, *Biosens. Bioelectron.*, 2010, **25**, 1735.
7. K. E. Toghill and R. G. Compton, *Int. J. Electrochem. Sci.*, 2010, **5**, 1246.
8. L. Meng, J. Jin, G. Yang, T. Lu, H. Zhang and C. Cai, *Anal. Chem.*, 2009, **81**, 7271.
9. S. Tominaka, Y. Nakamura and T. Osaka, *J. Power Sources*, 2010, **195**, 1054.
10. A. Pearson and A. P. O'Mullane, *Chem. Commun.*, DOI: 10.1039/C4CC09614B.
11. J. O'M. Bockris and S. U. M. Khan, in *Surface Electrochemistry*, Plenum Press, New York, 1993.
12. E. Antolini, *ACS Catal.*, 2014, **4**, 1426.
13. H. -B. Noh, K. -S. Lee, P. Chandra, M. -S. Won and Y. -B. Shim, *Electrochim. Acta*, 2012, **61**, 36.
14. R. Qiu, X. L. Zhang, R. Qiao, Y. Li, Y. I. Kim and Y. S. Kang, *Chem. Mat.*, 2007, **19**, 4174.
15. H. Fredriksson and U. Akerlind, in *Solidification and Crystallization Processing in Metals and Alloys*, Wiley, Stockholm, 2012.
16. A. J. Bard, G. Inzelt and F. Scholz, in *Electrochemical Dictionary*, Springer-Verlag, Heidelberg, 2012.
17. S. Gottsfeld and T. A. Zawodzinski, in *Advances in Electrochemical Science and Engineering*, ed. R. C. Alkire and D. M. Kolb, Wiley-VCH, Weinhim, 1997, vol. 5.
18. W. Ye, J. Yan, Q. Ye and F. Zhou, *J. Phys. Chem. C*, 2010, **114**, 15617.
19. J. F. Moulder, W. F. Stickle, P. E. Sobol and K. D. Bomben, in *Handbook of X-ray Photoelectron Spectroscopy*, Perkin-Elmer Corp., Eden Prairie, 1992, vol. 40.
20. K. Elouarzaki, A. L. Goff, M. Holzinger, J. Thery and S. Cosnier, *J. Am. Chem. Soc.*, 2012, **134**, 14078.

